Journal of Alloys and Compounds 488 (2009) 392–399

Contents lists available at ScienceDirect

Journal of Alloys and Compounds

journal homepage: www.elsevier.com/locate/jallcom

Corrosion behaviors of Mg and its alloys with different Al contents in a modified simulated body fluid

Zhaohui Wen[a], Changjun Wu[a,*], Changsong Dai[b], Feixia Yang[b]

[a] Department of Ultrasound, First Affiliated Hospital of Harbin Medical University, Harbin 150001, China
[b] School of Chemistry Engineering and Technology, Harbin Institute of Technology, Harbin 150001, China

ARTICLE INFO

Article history:
Received 3 July 2009
Received in revised form 30 August 2009
Accepted 31 August 2009
Available online 8 September 2009

Keywords:
Magnesium alloy
Biodegradability
Corrosion

ABSTRACT

The corrosion behaviors of pure magnesium (Mg) and three Mg alloys with different Al contents were investigated in a modified simulated body fluid (m-SBF) through immersion tests, Tafel experiments, and electrochemical impedance spectroscopic (EIS) experiments. The immersion results show that the corrosion rates (CRs) of the four samples were in an order of AZ91D < AZ61 < AZ31 < pure Mg after immersion for 1 day. With an increase in immersion time, their corrosion rates decreased and then a stable stage was reached after 16 days. The order of CRs of the four samples changed to AZ91D < pure Mg < AZ61 < AZ31 after immersion for 24 days. The results of EIS experiments indicate that the charge transfer resistance (R_{ct}) of the three magnesium alloys initially increased and then decreased while the R_{ct} of pure Mg was kept lower within 24 h. The results of a scanning electron microscopy (SEM) and energy dispersive spectroscopy (EDS) show that pure Mg and three alloys were heterogeneously corroded in the m-SBF. The corrosion of pure Mg, which showed a more uniform corrosion appearance, resulted from localized corrosion over the entire surface. Alloy AZ91D (of 8.5–9.5 wt.% Al) showed relatively uniform corrosion morphology and the β-$Mg_{12}Al_{17}$ precipitates in alloy AZ91D were more homogeneously and continuously distributed along the grain boundaries. Obvious corrosion pits were found on the surface of alloy AZ61 and AZ31. The corrosion pits of alloy AZ61 were shallower than those of alloy AZ31. Alloy AZ61 (of 5.8–7.2 wt.% Al) possessed more Al_8Mn_5 and a little β-$Mg_{12}Al_{17}$ presented along the grain boundary heterogeneously and discontinuously. Al_8Mn_5 was the main phase of the AZ31 alloy (of 2.5–3.5 wt.% Al) dispersed into the matrix. In conclusion, the microstructure and the Al content in the α-Mg (Al) matrix significantly affected the corrosion properties of the alloys in the m-SBF. With the increase in Al content, the corrosion resistances of the samples were improved.

1. Introduction

As innovative biodegradable metallic implant materials, magnesium and its alloys have gained special interest in medical applications in recent years [1]. Mg is an essential element to the human metabolism as a cofactor for many enzymes and a stabilizer for the structures of DNA and RNA [2]. The daily intake of Mg for a normal adult is about 300–400 mg and excess Mg cations can be gradually dissolved, absorbed, consumed or excreted in the human body. Moreover, owing to its degradability in human body fluids, repeated surgery is unnecessary to remove an implant made of Mg and thus physical irritation and chronic inflammatory reactions should be avoided [3–6]. In addition, the specific density, Young's modulus and yield strength of magnesium alloys are closer to those of human bones, which will avoid stress shielding [3–6].

Although a sufficient corrosion rate is important for implants to biodegrade in body fluid, applications of Mg implants are not common primarily because degradation rate of pure Mg is unacceptably high in at the pH level (7.4–7.6) of body fluid and high chloride environment of the physiological systems [7]. Hence, untreated magnesium implants cannot maintain sufficient mechanical integrity before the tissue has sufficiently healed [8–10].

There are two basic approaches to control the biodegradation rate: (1) surface treatment or application of a suitable coating on Mg alloys [6,11,12], and (2) modification of the alloy composition or microstructure, such as purification of Mg [3] and alloying Mg with other elements [8,13–15].

From a material science and engineering point of view, it is an important task to find the optimal alloy composition for degradable implants. The microstructure of the alloy composition, especially the amount and distribution of the intermetallic phases and the grain size, has shown an important influence on the corrosion behavior of Mg alloys [10,13,16]. Although the microstructure

* Corresponding author. Tel.: +86 451 85555905; fax: +86 451 53670428.
E-mail addresses: wucj163@126.com (C. Wu), changsd@hit.edu.cn (C. Dai).

0925-8388/$ – see front matter © 2009 Elsevier B.V. All rights reserved.
doi:10.1016/j.jallcom.2009.08.147

Table 1
Chemical compositions of pure Mg and three magnesium alloys.

Sample	Chemical compositions (wt.%)							
	Al	Zn	Mn	Cu	Ni	Fe	Si	Ca
Pure Mg	0	0	0	<0.00200	<0.00200	0.02000	0	0
AZ91D	8.60069	0.74184	0.24512	0.00313	0.00095	0.00392	0.07509	0.00038
AZ61	6.02190	0.62998	0.29424	0.00216	0.00081	0.00384	0.01588	0.00026
AZ31	2.73661	0.75291	0.29385	0.00161	0.00082	0.00345	0.02291	0.00015

of the corrosion process of some Mg alloys in corrosive solutions has been understood, little has been investigated about the influence of their amount and distribution of the intermetallic phases on biodegradation performance under physiological conditions. Particularly, the effect of alloying elements such as Al on the in vitro degradation behavior is still unclear. It is possible to approximate in vitro the corrosion process that these alloys will undergo in vivo. This may not only provide instruction on the future selection of the preferable alloying elements for implant applications, but also direct the future composition design of the biodegradable magnesium alloy systems. In the present paper, preliminary results on this promising topic are reported.

2. Experimental details

Commercial pure Mg and magnesium alloys AZ31, AZ61 and AZ91D (Baoding Dong Qi Magnesium Alloy Products Co., Ltd, Shenzhen, China) were used in this study. Nomenclature of the samples was used according to the American Society for Testing and Materials (ASTM) standard [17]. Their nominal compositions (wt.%) are listed in Table 1. The samples were cut into 10 mm × 10 mm × 10 mm and 10 mm × 10 mm × 5 mm coupons for the immersion test and the electrochemical test, respectively.

In this study, the in vitro immersion test was carried out in a modified simulated body fluid (m-SBF), which was maintained at the most common body temperature of 36.5 ± 0.5 °C. The composition of the m-SBF is given in Table 2 [18]. The solution was buffered with 2-(4-(2-hydroxyethyl)-1-piperazinyl) ethanesulfonic acid (HEPES) to a physiological pH of 7.4.

For the immersion test, the coupons were polished with SiC paper up to 1000 grit, ultrasonically rinsed in acetone for 10 min, dried in warm flowing air and then weighed by a balance with an accuracy of 0.1 mg. Then the samples were immersed in the m-SBF for 1, 2, 5, 8, 16, 20 and 24 days. At each time point, the samples were removed from the m-SBF, rinsed with de-ionized water, dried in warm flowing air and then weighed. The mass variation was calculated (mass variation = (mass before immersion − mass after immersion)/surface area) and then the samples were immersed in a solution comprising 200 g L^{-1} CrO_3 and 19 g L^{-1} $AgNO_3$ for 10–15 min to remove the corrosion products. After that, they were quickly cleaned with distilled water, dried in warm flowing air and weighed for the final weight (mass loss = (mass before immersion − mass after cleaning in chromic acid)/surface area). Three parallel immersion tests were carried out for an average result.

The corrosion rate (CR) of the samples was calculated via the following equation [19]

$$\mathrm{CR(mm/yr)} = \frac{tW}{ATρ}10 \quad (1)$$

where t is 365 × 24(h), W is the mass loss (g), A is the original surface area exposed to the corrosive media (cm^2), T is the immersion time (h) and $ρ$ is the sample standard density (g/cm^3) (pure Mg, 1.74 g/cm^3; AZ31, 1.77 g/cm^3; AZ61, 1.78 g/cm^3; AZ91D, 1.83 g/cm^3).

Table 2
Chemical composition of the m-SBF [18].

Reagent	Amount
NaCl (g L^{-1})	5.403
$NaHCO_3$ (g L^{-1})	0.504
Na_2CO_3 (g L^{-1})	0.426
KCl (g L^{-1})	0.225
$K_2HPO_4·3H_2O$ (g L^{-1})	0.230
$MgCl_2·6H_2O$ (g L^{-1})	0.311
0.2 M NaOH (mL L^{-1})	100.00
HEPES[a] (g L^{-1})	17.892
$CaCl_2$ (g L^{-1})	0.293
Na_2SO_4 (g L^{-1})	0.072
1 M NaOH (mL L^{-1})	15.00

[a] HEPES = 2-(4-(2-hydroxyethyl)-1-piperazinyl) ethanesulfonic acid.

After the samples were mounted in epoxy-resin with only one surface of 1 cm^2 exposed, the samples were polished with SiC paper up to 1000 grit, washed with distilled water and ultrasonically cleaned in acetone prior to the tests. The polarization experiments were performed using a Model 273 potentiostat (made by EG&G Princeton Applied Research). The electrochemical impedance spectroscopy (EIS) tests were carried out under different conditions at 37 ± 0.5 °C using a Model 273 potentiostat, a 5210 phase-lock amplifier, a NEC Power mate ITX computer system, and an EG&G M 398 EIS testing system in a range of 0.1 Hz to 10 kHz. The experimental setup was a standard three-electrode system with the sample as the working electrode, a saturated calomel electrode (SCE) as the reference electrode, and a platinum mesh as the counter electrode. The results of the measurements were analyzed by using the EG&G EQUIVCRT software. Prior to the beginning of the polarization and EIS experiments, the samples were first immersed in a beaker open to air containing the m-SBF maintained at 37 °C for 1 h to establish a relatively stable free corrosion potential. The sweep rate of the polarization curve measurement was 0.5 mV s^{-1}. The corrosion current density (i_{corr}) was converted into the corrosion rate according to the Faraday's Law

$$\mathrm{CR(mm/yr)} = \frac{Mti_{corr}}{nFρ}10 \quad (2)$$

where CR is the corrosion rate, M is the molar mass (magnesium 24.31 g/mol), t equals to 3600 × 24 × 365(s), i_{corr} is the corrosion current density(A/cm^2), n is the number of electrons involved in the corrosion reaction, F is the Faraday's constant (96 485 A s/mol) and $ρ$ is the sample standard density (g/cm^3).

After the specified immersion time, the surface morphology and the chemical compositions of the samples were examined with a scanning electron microscopy (SEM, HITACHI S-570, S-4700, Japan) equipped with energy dispersive spectroscopy (EDS).

3. Results and discussion

3.1. Immersion tests

Fig. 1 shows mass changes of pure Mg and three magnesium alloys immersed in the m-SBF for different times before and after cleaning of the surfaces in chromic acid.

It was observed that the plot of the mass loss showed the same tendency as the mass variation. Alloy AZ31 and pure Mg had the largest mass increases of about 1.61 mg/cm^2 and 1.55 mg/cm^2, respectively, after immersion for 1 day. Then the masses of AZ31 and pure Mg continued to increase from the 2 days to the 24 days while dramatic decrease occurred from 16 to 20 days. After immersion for 24 days, the total mass variations of alloy AZ31 and pure Mg were 14.26 mg/cm^2 and 5.45 mg/cm^2, respectively (Fig. 1(a)). The mass losses of alloy AZ31 and pure Mg were about 4.02 mg/cm^2 and 3.82 mg/cm^2 after immersion for 1 day, and about 23.24 mg/cm^2 and 14.26 mg/cm^2 after immersion for 24 days, respectively (Fig. 1(b)). Although alloy AZ91D had the same tendency as pure Mg and alloy AZ31 before and after the corrosion products were removed, the mass variation and mass loss of alloy AZ91D were only 0.19 mg/cm^2 and 1.55 mg/cm^2, respectively, which were much less than that of the pure Mg after immersion for 1 day. However, the mass variation and mass loss of alloy AZ91D reached about 4.61 mg/cm^2 and 14.51 mg/cm^2, respectively, after immersion for 24 days, which were similar to those of the pure Mg (Fig. 1(a) and (b)). The mass variation and the mass loss of AZ61 were about 0.77 mg/cm^2 and 3.18 mg/cm^2 after 1 day of immersion, and then they were continuously increasing till the end of the immersion test, which was different from the behavior of the

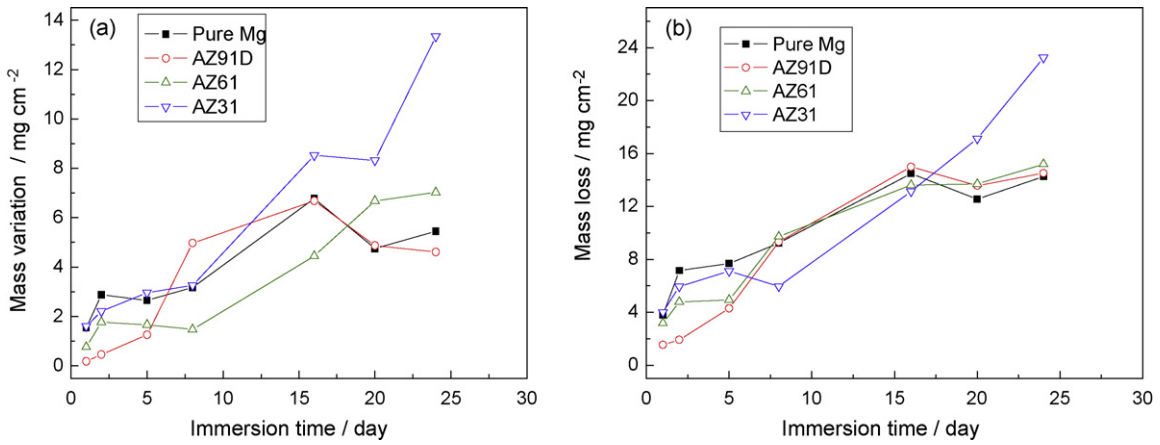

Fig. 1. (a) Mass variations of pure Mg and three Mg alloys immersed in the m-SBF for different time before immersion in chromic acid. (b) Mass losses of pure Mg and three Mg alloys immersed in the m-SBF for different time after cleaning of the surface in chromic acid.

above-mentioned samples. The final mass variation and mass loss of alloy AZ61 were 7.02 mg/cm^2 and 15.20 mg/cm^2, respectively (Fig. 1).

In conclusion, the mass variation and the mass loss of four samples could be ranked in the following order: AZ91D < AZ61 < AZ31 < pure Mg after immersion for 2 days. The order then changed and the final order was AZ91D < pure Mg < AZ61 < AZ31 after 24 days of immersion.

Fig. 2 shows the mass variation rates of pure Mg and three Mg alloys immersed in the m-SBF for different time before immersion in chromic acid. The AZ31 alloy and pure Mg showed high mass variation rates, about 0.0700 mg/(cm^2 h) and 0.0600 mg/(cm^2 h) after immersion for 1 day, respectively, and then the rates decreased rapidly and reached a stable stage after about 8 days of immersion. After immersion for 24 days, the mass variation rates of the AZ31 alloy and pure Mg were about 0.0231 mg/(cm^2 h) and 0.0095 mg/(cm^2 h), respectively. The mass variation rate of the AZ61 alloy showed the same tendency as those of the above-mentioned two samples except that lower mass variation rates after immersion for 1 and 24 days, about 0.0300 mg/(cm^2 h) and 0.0100 mg/(cm^2 h), respectively, could be observed (Fig. 2). Compared with the above samples, the AZ91D alloy showed the most stable and lowest mass variation rate, which was about 0.0078 mg/(cm^2 h) after 1 day of immersion. This value was just slightly lower than that after immersion for 24 days, which was about 0.0080 mg/(cm^2 h) (Fig. 2). Accordingly, the mass variation rates of four samples were in an increasing order: AZ91D < AZ61 < AZ31 < pure Mg for the first 5 days of immersion and it became AZ91D < pure Mg < AZ61 < AZ31 after immersion for 24 days.

Fig. 3 shows CRs of pure Mg and three Mg alloys in the immersion test for different time lengths. The conversion of the mass loss into corrosion rates Eq. (1) revealed that the CRs of all the samples decreased with immersion time increasing from 1 to 8 days and then became stable. The AZ31 alloy and pure Mg had high CRs of about 8.290 mm/year and 8.008 mm/year after immersion for 1 day, and then the CRs decreased rapidly after about 8 days of immersion. After immersion for 24 days, the CRs of the AZ31 alloy and pure Mg were 1.997 mm/year and 1.218 mm/year, respectively. The CR of sample AZ61 had the same tendency as the above two samples except that it had a very low corrosion rate of about 6.510 mm/year after 1 day of immersion and 1.299 mm/year after immersion for 24 days. Compared with other samples, sample AZ91D had the most stable and lowest corrosion rate. After 1 day of immersion, the CR of sample AZ91D was about 3.086 mm/year, which was just slightly higher than that of 1.206 mm/year after immersion 24 days. Consequently, the CRs of four samples were in an order of AZ91D < AZ61 < AZ31 < pure Mg for the first 5 days of immersion and the order became AZ91D < pure Mg < AZ61 < AZ31 after 24 days of immersion.

3.2. Electrochemical testing

Fig. 4 shows the Nyquist plots of pure Mg and three magnesium alloys after immersion in the m-SBF for 1, 2, 6, 12 and 24 h. The Nyquist plots consisted of one capacitive loop in the high frequency

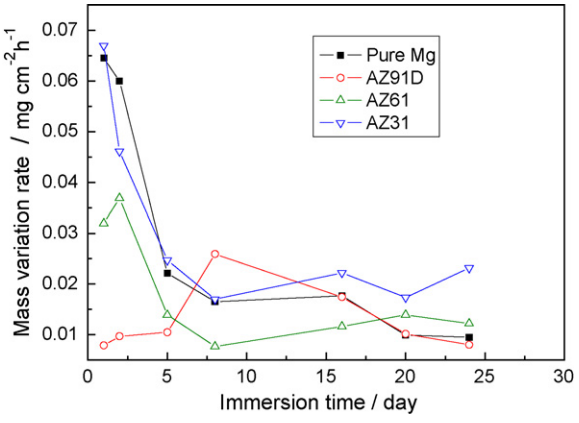

Fig. 2. Mass variation rates of pure Mg and three Mg alloys immersed in the m-SBF for different time before immersion in chromic acid.

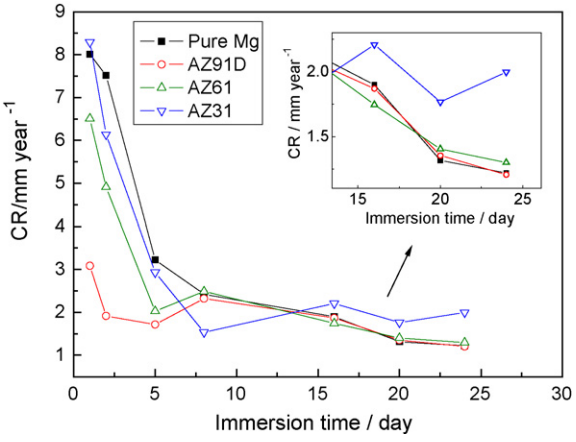

Fig. 3. CRs of pure Mg and three Mg alloys in immersion test for different time.

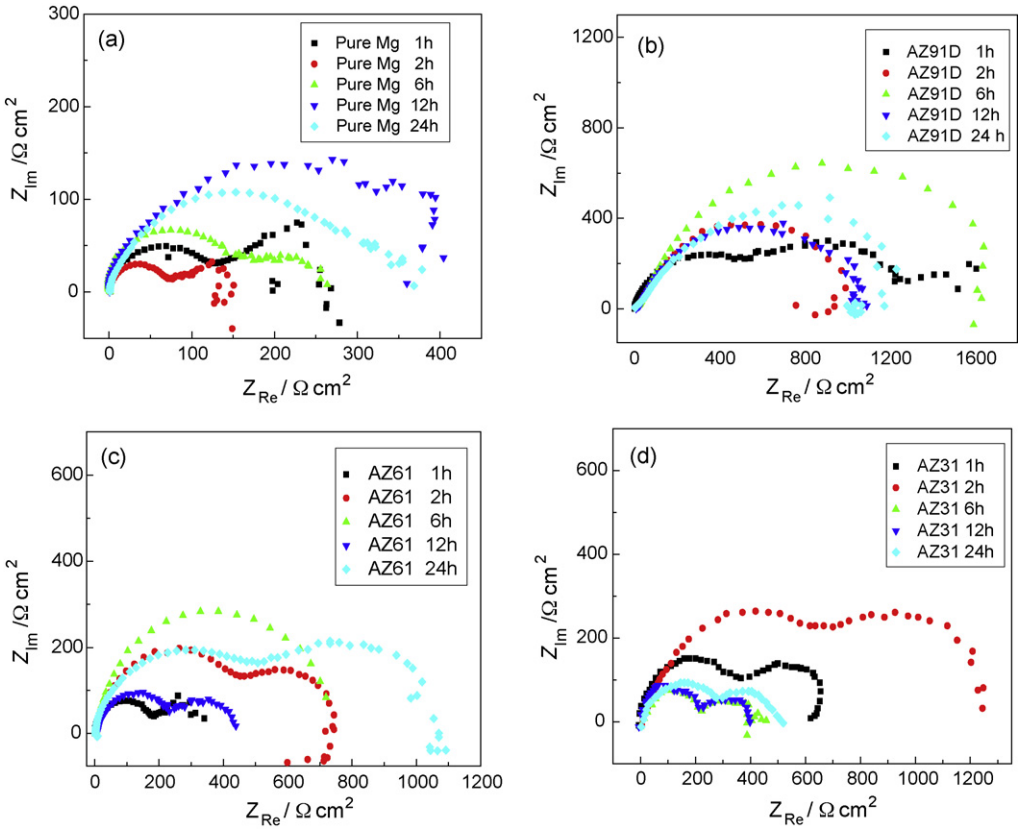

Fig. 4. The Nyquist plots of pure Mg and three Mg alloys after immersion in the m-SBF at 37 °C for 1, 2, 6, 12 and 24 h: (a) pure Mg, (b) AZ91D, (c) AZ61 and (d) AZ31.

range (one time constant) or two capacitive loops in the high frequency range and the low frequency range (two time constants). There was also an inductance loop in the low frequency range sometimes involved in the spectra. The diameter of the capacitive loop in the high frequency range represented the charge transfer resistance (R_{ct}). The R_{ct} value reflected how difficult the electrochemical corrosion reaction might be. The diameter of the capacitive loop in the low frequency range reflected the surface film resistance (R_s) which corresponded with the thickness and integrity of the corrosion film [20]. The inductance loop in the lower frequency range was related to the breakdown of the surface film or relaxation of adsorbed species, such as $Mg(OH)_{ads}$ or $Mg(OH)_2$ [21,22], which is taken as an indication of pitting corrosion [23,24].

The corresponding R_{ct} values of four samples after immersion in the m-SBF for 1, 2, 6, 12 and 24 h extracted from Fig. 4 are given in Fig. 5. It was observed that R_{ct} values of the three magnesium alloys initially increased and then decreased, while, the values of pure Mg were kept lower than the other samples within 24 h. The variation of R_{ct} was related to the dynamic process of the growth, crack or stripping of the corrosion film [10]. It could be deduced that a vigorous corrosion reaction occurred between Mg and the m-SBF. After immersion into m-SBF, the R_{ct} of AZ91D increased sharply due to the fast formation of a corrosion product layer. After immersion for 6 h, with the growth continued, the cracks and the stripping increased rapidly from 6 to 12 h and then increased slowly. Therefore, the R_{ct} of AZ91D was shown decreased rapidly from 6 to 12 h and then decreased slowly. As those of the AZ91D, the R_{ct} of AZ61 alloy showed the same tendency within 12 h, and then increased again which might be due to the growth suppressed the stripping again. However, the highest R_{ct} of AZ31 was shown after immersion for 2 h, and then it decreased until a stable stage was reached after 6 h of immersion. Different from R_{ct} for the above samples, the R_{ct} value of pure Mg became the lowest after immersion for 2 h and then kept stale without obvious change. The formation of stable stage might be due to the dynamic equilibrium among the growth, crack or stripping rate. Fig. 5 also shows that the R_{ct} of the four alloys can be put into the following order: AZ91D > AZ61 > AZ31 > pure Mg after immersion for 24 h. These results are consistent with their corrosion rates as shown in Fig. 3.

Tafel plots of pure Mg and three kinds of magnesium alloy after immersion in the m-SBF for 16 and 24 days are shown in Fig. 6.

The corresponding electrochemical parameters extracted from these curves are given in Table 3. From Table 3, it could be observed that the E_{corr} values of the four samples shifted in the negative direction after immersed in the m-SBF from 16 to 24 days. However, i_{corr} showed little difference between 16 and 24 days, which shows that the corrosion rates of the samples went stable. This result is in accordance with Fig. 3. From the result of Table 3, it could also

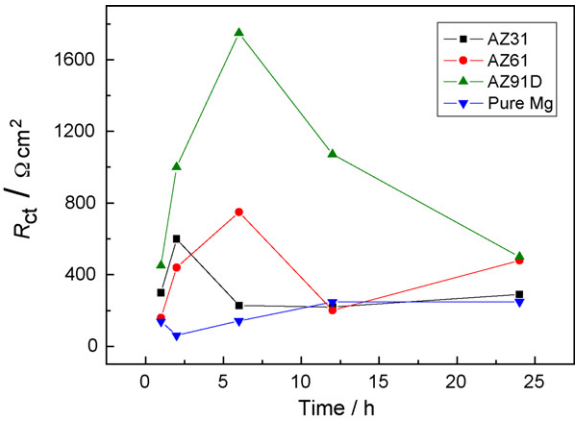

Fig. 5. The R_{ct} of four samples after immersion in the m-SBF for 1, 2, 6, 12 and 24 h.

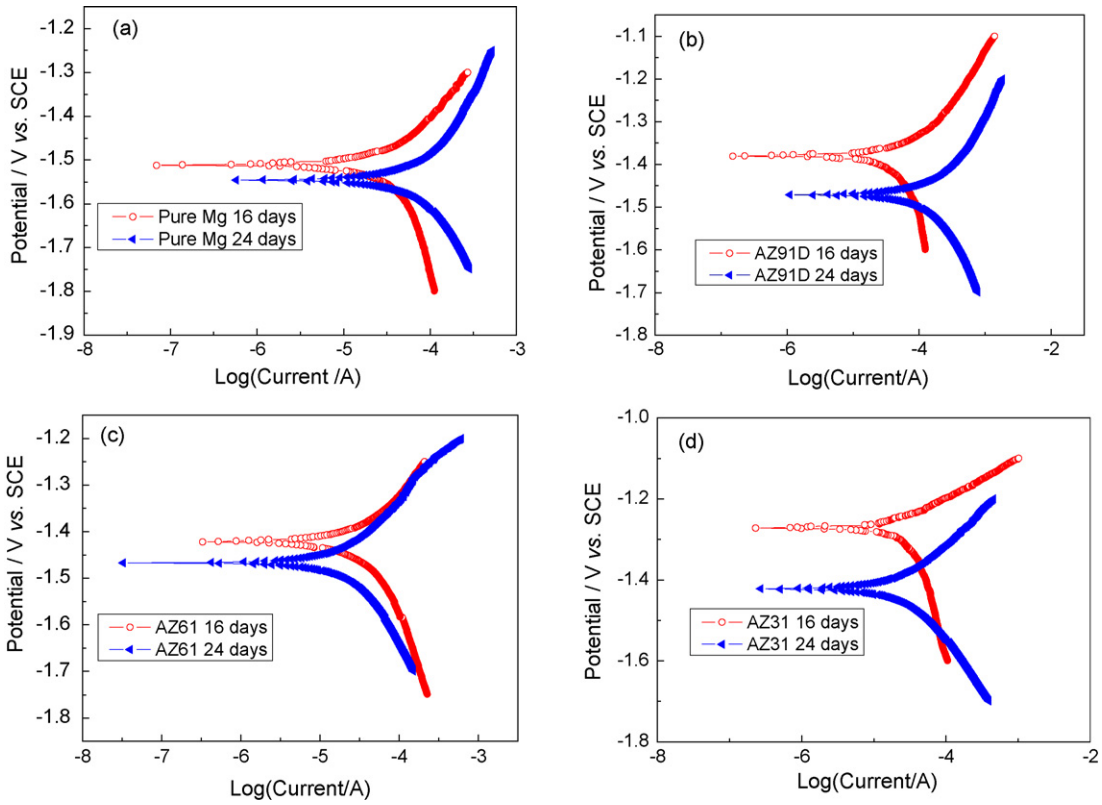

Fig. 6. The Tafel plots of four samples after immersion in the m-SBF at 37 °C for 16 and 24 days: (a) pure Mg, (b) AZ91D, (c) AZ61 and (d) AZ31.

Table 3
Results of Tafel curves of four samples after immersion in the m-SBF for 16 and 24 days.

Sample	Pure Mg		AZ91D		AZ61		AZ31	
	16 d	24 d	16 d	24 d	16 d	24 d	16 d	24 d
E_{corr}/V (vs. SCE)	−1.513	−1.547	−1.456	−1.472	−1.423	−1.468	−1.273	−1.423
i_{corr} (A cm^{-2})	3.005e-5	8.046e-5	1.190e-4	1.417e-4	3.255e-5	2.272e-5	3.274e-5	2.319e-5
CR[a] (mm yr^{-1})	0.686	1.837	2.583	3.076	0.726	0.507	0.735	0.521

[a] CR calculated according to Eq. (2).

be observed that i_{corr} values of four samples were in an order of AZ91D > pure Mg > AZ31 > AZ61 after immersion in the m-SBF for 16 and 24 days, which is not in accordance with Fig. 3. The main reason was that Tafel plots could be employed to study the corrosion rate of the uniform corrosion attack instead of nonuniform corrosion.

3.3. Surface morphology

The SEM images of four samples in Fig. 7 were taken after immersion in the m-SBF for different time lengths. EDS analysis was conducted on several small surface areas and the element quantitative analysis results are listed in Table 4. It was observed that the surfaces of four samples were first covered by a corrosion layer with many cracks. Ca and P components were found in the corrosion layer, especially in the corrosion areas (see Table 4). With the increase in time, the layer became thicker and thicker. EDS analysis of the $Mg(OH)_2$ layer showed that Ca and P were hardly detected (Fig. 8). This suggested that the $Mg(OH)_2$ layer formed on the surface of the samples might act as a barrier to prevent magnesium from further absorbing Ca and P from the m-SBF. However, the $Mg(OH)_2$ film was unstable in the presence of aggressive ions like chloride and in acidic solutions. The cracking and curling of the $Mg(OH)_2$ films on Mg samples was attributed to the layered structure, which facilitated easy basal cleavage, as well as a P-B (Pilling-Bedworth) ratio of 1.77, which resulted in compressive internal stress. After 5 days of immersion the appearances of three alloys began to be covered with many pits with different depths and sizes except for pure Mg. At the same time some needle-shaped clusters began to form on the samples' surfaces especially on the corroding area and some fell off from the surface with time increasing (Fig. 9). The corrosion of pure Mg, which showed more uniform corrosion appearance, resulted from localized corrosion over the entire surface. The localized corrosion on pure Mg was different from the auto-catalyzed pitting [25]. The corrosion reaction on the surface of the AZ31 alloy was the most intensive of the four samples. The corrosion pits on alloy AZ61 were shallower than those on alloy AZ31. The pits on alloy AZ91D were less and shallower

Table 4
EDS analysis results on the surface reaction layer of four samples immersed in the m-SBF for 24 h.

Sample	Element percent (at.%)				
	Mg	Ca	P	Al	Cl
Pure Mg	66.18	11.38	16.34	0	5.03
AZ91D	32.65	20.38	23.91	19.36	1.04
AZ61	32.92	24.73	23.89	15.13	2.92
AZ31	45.89	18.58	24.04	6.17	2.31

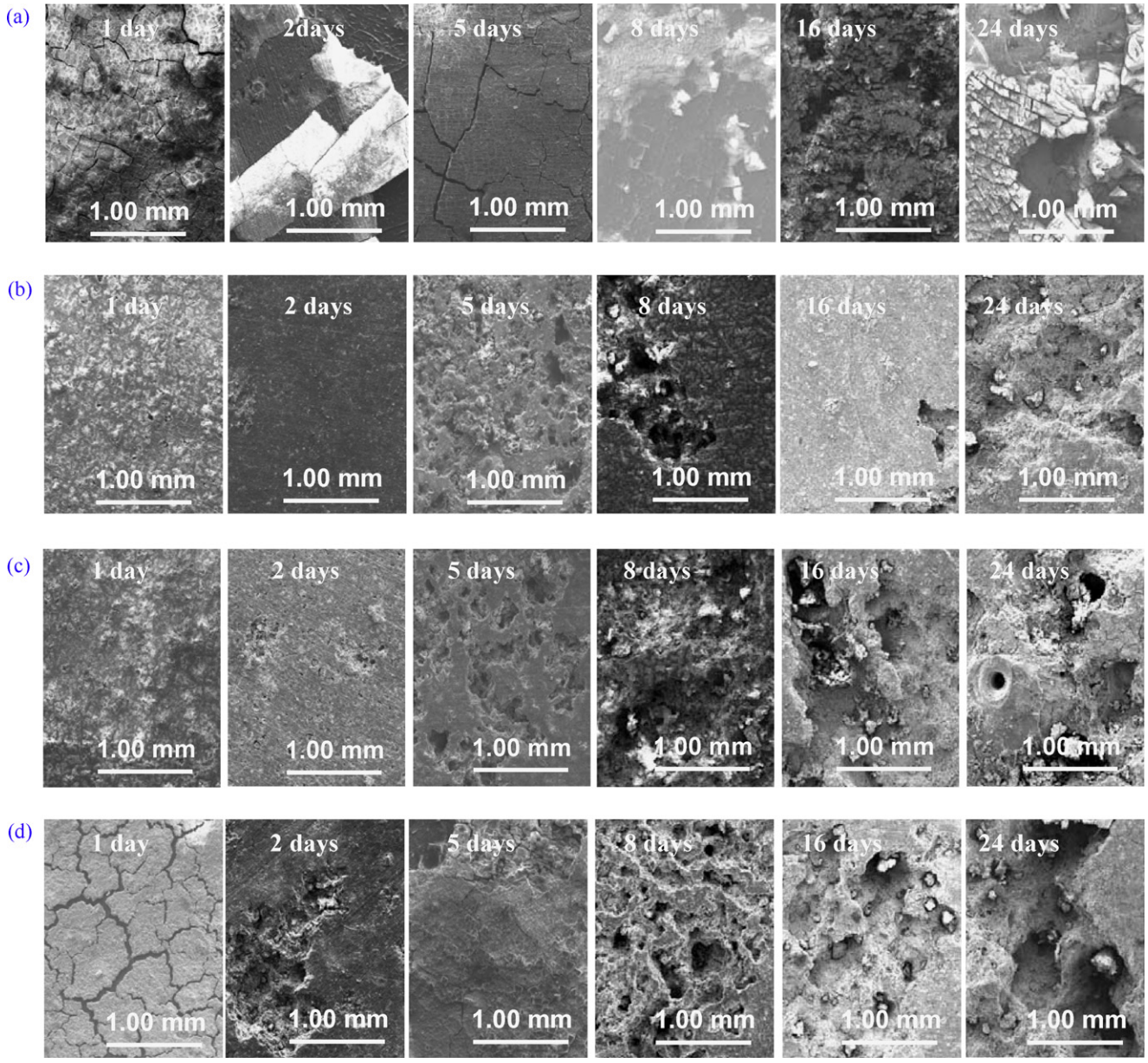

Fig. 7. SEM micrographs of four samples after immersion in the m-SBF for different time: (a) pure Mg, (b) AZ91D, (c) AZ61 and (d) AZ31.

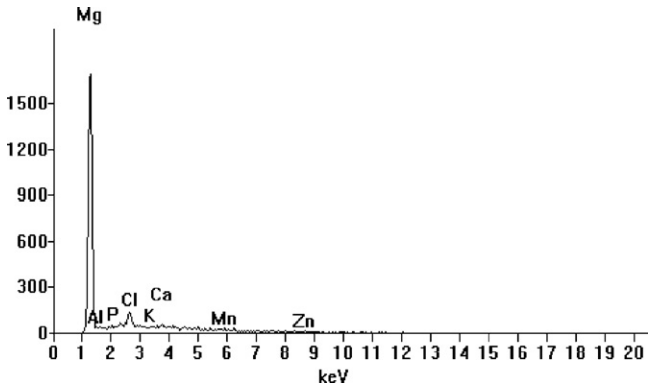

Fig. 8. EDS of pure Mg immersed in the m-SBF for 8 days.

than those on the other two alloys. These results are consistent with their corrosion rates as shown in Fig. 3. Combined with the results of Figs. 2–5, it could be deduced that a vigorous reaction between Mg and the m-SBF resulted in fast corrosion of magnesium and fast formation of a corrosion product layer on the surface. Within 5 days, the reaction suppressed the precipitation gradually on the surface and after that, a stable stage was reached (Figs. 2–4, Table 2).

As the aluminum-containing alloy, AZ magnesium alloys possessed different electrochemical and corrosion properties. The microstructure and the Al content in the α-Mg (Al) matrix tended to influence the corrosion properties [26,27]. Fig. 10 shows SEM micrographs of three alloys with the surfaces being cleaned in chromic acid after immersion into the m-SBF for 24 days. EDS data are shown in Table 5. After the corrosion products were removed, the AZ31 alloy (2.5–3.5 wt.% Al) suffered from the most intensive localized corrosion attack (Fig. 10(a)). At higher magnifications, some twig-like and plate-like matrices were observed (Fig. 10(b)). It was accepted that for a solid aluminum in the matrix, the content

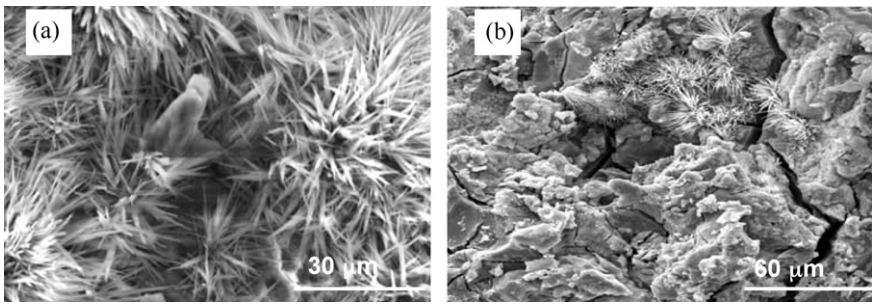

Fig. 9. Needle-like clusters on the corroded surface of (a) pure Mg and (b) AZ91D alloy.

of solid Al may be varied from about 20 wt.% in the vicinity of β-phase to 1.5 wt.% in the grain centre [28]. The EDS analysis showed that the twig-like matrix was rich in the Al_8Mn_5 phase and α-Mg (point 3 of Fig. 10(b), Table 5) and the other matrix was rich in α-Mg (points 1 and 2 of Fig. 10(a), Table 5). It was accepted that when the contents of Al element were more than 2 wt.%, a matrix of α grains with the β-phase (the intermetallic $Mg_{17}Al_{12}$) along the α grain boundaries could be observed in AZ magnesium alloys [23]. However, in this study, the β-$Mg_{12}Al_{17}$ phase was too little to be detected in AZ31 alloy because of the low content of Al in the alloy. Because the corrosion potential of Al–Mn was higher in comparison with other particles in the Mg–Al alloys [29,30], the area near the Al–Mn particles seemed to have undergone higher dissolution. The corrosion rate of alloy AZ31 was the highest of the four samples (Figs. 2 and 3). This was because that the Al_8Mn_5 phase only acted as a galvanic cathode to accelerate the corrosion of the α matrix [31].

As shown in Fig. 10(c), the micrographs of alloy AZ61 were similar to that of alloy AZ31. At higher magnifications, the un-attacked continuous network and the twig-like matrix could be observed (Fig. 10(d)). The EDS analysis showed that the twig-like matrix was rich in Al_8Mn_5 with a little $Mg_{12}Al_{17}$ (point 6 of Fig. 10(d) and Table 5) and the other matrix was rich in α-Mg with a little $Mg_{12}Al_{17}$ (points 4 and 5 of Fig. 10(c) and Table 5). The AZ61 alloy seemed to have undergone slightly lower dissolution in comparison with the AZ31 alloy (Fig. 10(c)). The corrosion rate of alloy AZ61 in the m-SBF was lower than that of alloy AZ31 (Figs. 2 and 3). The possible explanation for that was with the increase of the content of Al, alloy AZ61 (5.8–7.2 wt.% Al) possessed more Al_8Mn_5 and only a little β-$Mg_{12}Al_{17}$ presented along the grain boundary heteroge-

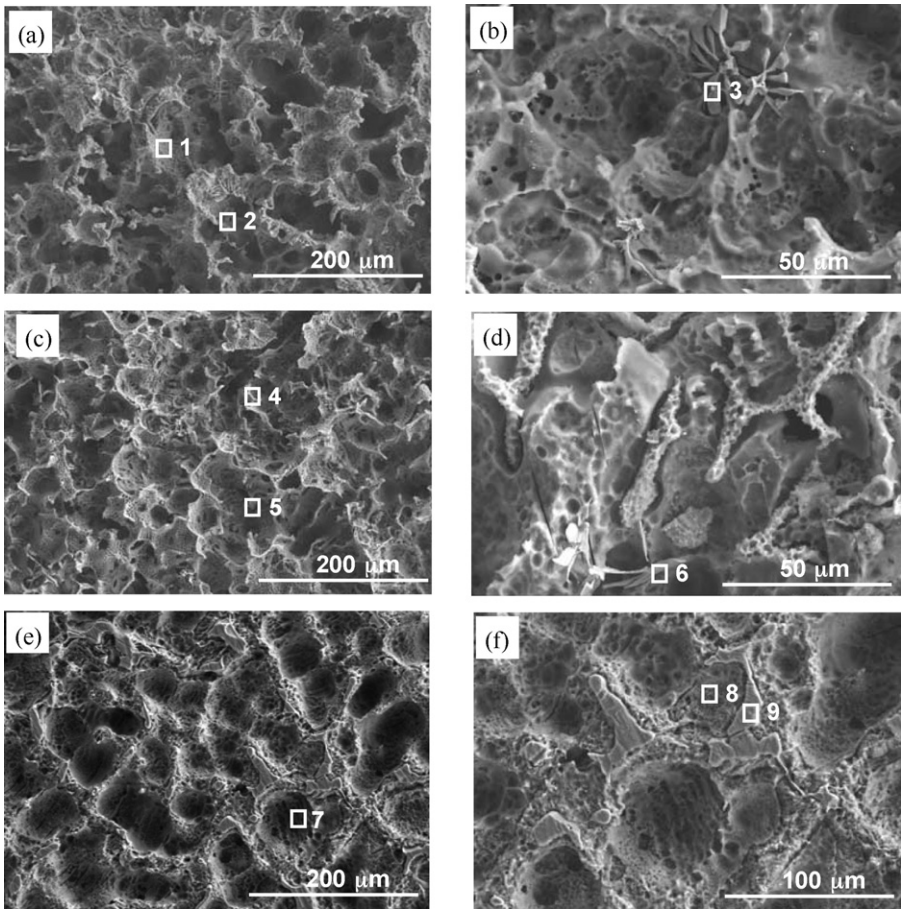

Fig. 10. SEM micrographs of three magnesium alloys with the surfaces being cleaned in chromic acid after immersion into the m-SBF for 24 days: (a) and (b) AZ31, (c) and (d) AZ61, (e) and (f) AZ91D.

Table 5
Quantitative EDX data of the three alloys with the surfaces being cleaned in chromic acid after immersion into the m-SBF for 24 days.

Sample	Point	Element percent (wt.%)				Phase
		Mg	Al	Mn	Zn	
AZ31	1	81.18	05.38	02.47	04.65	α
	2	86.05	05.45	00.55	02.67	α
	3	39.57	26.60	29.25	01.18	$\alpha + Al_8Mn_5$
AZ61	4	65.07	16.58	02.13	05.69	$\alpha + Mg_{12}Al_{17}$
	5	61.44	22.27	00.65	07.19	$\alpha + Mg_{12}Al_{17}$
	6	9.54	34.84	35.47	02.72	$Al_8Mn_5 + Mg_{12}Al_{17}$
AZ91D	7	80.39	08.94	01.40	02.85	α
	8	83.89	07.56	00.83	02.18	α
	9	51.55	35.69	00.50	05.95	$\alpha + Mg_{12}Al_{17}$

neously and discontinuously. The barrier effect of the β-phase of AZ61 might be stronger to impede corrosion.

After the corrosion was removed, many circle-like pits could be seen on the surface of alloy AZ91D in Fig. 10(e). At higher magnifications, the grain boundaries appeared protruding and a shallow pit of the matrix was observed (Fig. 10(f)). The EDS analysis showed that the protruded matrix was rich in $Mg_{12}Al_{17}$ (point 9 of Fig. 10(f) and Table 5) while the other matrix was rich in α-Mg (point 7 and 8 of Fig. 10(e), (f) and Table 5). The matrix rich of Al formed a broad continuous grain-boundary barrier and the area near these particles seemed to have undergone slightly higher dissolution (Fig. 10(e) and (f)). It was shown that the dissolution tendency of the matrix left relatively stable grain boundaries, which might act as a barrier to protect the matrix from dissolution (Fig. 10(e)). Combined with the results of polarization curves it could be seen that the corrosion morphology was a more nonuniform corrosion damage than a uniform corrosion damage (Fig. 6 and Table 3). The β-precipitates in alloy AZ91D (8.5–9.5 wt.% Al) were more homogeneously and continuously distributed along the grain boundaries, so the barrier effect of the β-phase was evident to stop corrosion (Fig. 10(e) and (f)) [28,32].

4. Conclusions

In summary, there was a vigorous reaction between Mg and the m-SBF. The immersion test and electrochemical test showed that the CRs of the four samples was in an order of AZ91D < AZ61 < AZ31 < pure Mg after immersion for 24 h. The immersion test also showed that the corrosion rates of the samples decreased with the increase in immersion time and the order of corrosion resistance of the four samples became AZ91D > pure Mg > AZ61 > AZ31 after immersion for 24 days. Pure Mg and three Mg alloys heterogeneously corroded in the m-SBF. The corrosion of pure Mg, which showed more uniform corrosion appearance, resulted from localized corrosion over the entire surface. For the aluminum-containing alloys, the corrosion originated from grain boundaries. Alloy AZ91D showed relatively uniform corrosion morphology with a few shallow pits. The obvious corrosion pits were found on the surface of alloys AZ61 and AZ31. The corrosion pits of alloy AZ61 were shallower than those of alloy AZ31. Accordingly, the microstructure and the Al content in the α-Mg (Al) matrix significantly affected their corrosion properties in the m-SBF. With the Al content increasing, the corrosion resistances of the samples were improved.

References

[1] G.L. Song, S.Z. Song, Adv. Eng. Mater. 9 (2007) 298–302.
[2] A. Hartwig, Mutat. Res./Fund. Mol. Mech. Mutagen 475 (2001) 113–121.
[3] G.L. Song, Corr. Sci. 49 (2007) 1696–1701.
[4] F. Witte, V. Kaese, H. Haferkamp, E. Switzer, A. Meyer-Lindenberg, C.J. Wirth, H. Windhagen, Biomaterials 26 (2005) 3557–3563.
[5] C.E. Wen, M. Mabuchi, Y. Yamada, K. Shimojima, Y. Chino, T. Asahina, Scripta Mater. 45 (2001) 1147–1153.
[6] J. Lévesque, H. Hermawan, D. Dubé, D. Mantovani, Acta Biomater. 4 (2008) 284–295.
[7] M.P. Staiger, A.M. Pietak, J. Huadmai, G. Dias, Biomaterials 27 (2006) 1728–1734.
[8] M. Bobby Kannan, R.K. Singh Raman, Biomaterials 29 (2008) 2306–2314.
[9] Z.J. Li, X.N. Gu, S.Q. Lou, Y.F. Zheng, Biomaterials 29 (2008) 1329–1344.
[10] P. Shi, W.F. Ng, M.H. Wong, F.T. Cheng, J. Alloys Compd. 469 (2009) 286–292.
[11] L.P. Xu, F. Pan, G.N. Yu, L. Yang, E.L. Zhang, K. Yang, Biomaterials 30 (2009) 1512–1523.
[12] W. Shang, B.Z. Chen, X.C. Shi, Y. Chen, X. Xiao, J. Alloys Compd. 474 (2009) 541–545.
[13] H. Wang, Y. Estrin, H.M. Fu, G.L. Song, Z. Zúberová, Adv. Eng. Mater. 9 (2007) 967–972.
[14] X.N. Gu, Y.F. Zheng, Y. Cheng, S.P. Zhong, T.F. Xi, Biomaterials 30 (2009) 484–498.
[15] A.D. Südholz, N. Birbilis, C.J. Bettles, M.A. Gibson, J. Alloys Compd. 471 (2009) 109–115.
[16] M. Alvarez-Lopez, M. Dolores Pereda, J.A. del Valle, M. Fernandez-Lorenzo, M.C. Garcia-Alonso, O.A. Ruano, M.L. Escudero, Acta Biomater. (2009) doi:10.1016/j.actbio.2009.04.041.
[17] ASTM B 275-90: Standard practice for codification of certain nonferrous metals and alloys, cast and wrought. Annual Book of ASTM Standards, American Society for Testing and Materials, Philadelphia, Pennsylvania, USA, 1990.
[18] T. Kokubo, H. Takadama, Biomaterials 27 (2006) 2907–2915.
[19] ASTM-G31-72: Standard Practice for Laboratory Immersion Corrosion Testing of Metals. Annual Book of ASTM Standards.
[20] F. Zucchi, V. Grassi, A. Frignani, C. Monticelli, G. Trabanelli, J. Appl. Electrochem. 36 (2006) 195–204.
[21] G. Song, A. Atrens, D. St John, X. Wu, J. Nairn, Corros. Sci. 39 (1997) 1981–2004.
[22] G. Baril, N. Pébère, Corros. Sci. 43 (2001) 471–484.
[23] S. Jin, S. Amira, E. Ghali, Adv. Eng. Mater. 9 (2007) 75–83.
[24] J. Chen, J. Wang, E. Han, J. Dong, W. Ke, Electrochim. Acta 52 (2007) 3299–3309.
[25] G.L. Song, A. Atrens, Adv. Eng. Mater. 5 (2003) 837–858.
[26] F. Rosalbino, E. Angelini, S. De Negri, A. Saccone, S. Delfino, Intermetallics 13 (2005) 55–60.
[27] G. Song, A. Atrens, X. Wu, B. Zhang, Corros. Sci. 40 (1998) 1769–1791.
[28] G.L. Song, Adv. Eng. Mater. 7 (2005) 563–586.
[29] R.C. Zeng, J. Zhang, W.J. Huang, W. Dietzel, K.U. Kainer, C. Blawert, W. Kei, Trans. Nonferr. Met. Soc. China 16 (2006) s763–s771.
[30] G. Ben-Hamu, D. Eliezer, C.E. Cross, Th. Böllinghaus, Mater. Sci. Eng. A 452–453 (2007) 210–218.
[31] G.B. Hamu, D. Eliezer, L. Wagner, J. Alloys Compd. 468 (2009) 222–229.
[32] F. Witte, F. Feyerabend, P. Maier, J. Fischer, M. Störmer, C. Blawert, W. Dietzel, N. Hort, Biomaterials 28 (2007) 2163–2174.